Size effects on silver nanoparticles' properties

To cite this article: F D Kiss *et al* 2011 *Nanotechnology* **22** 275708

View the article online for updates and enhancements.

You may also like

- SPARC: MASS MODELS FOR 175 DISK GALAXIES WITH *SPITZER* PHOTOMETRY AND ACCURATE ROTATION CURVES
Federico Lelli, Stacy S. McGaugh and James M. Schombert
- Review—From Nano Size Effect to In Situ Wrapping: Rational Design of Cathode Structure for High Performance LithiumSulfur Batteries
Hongwei Chen, Yanbin Shen, Changhong Wang et al.
- Magnetization dynamics, throughput and energy dissipation in a universal multiferroic nanomagnetic logic gate with fan-in and fan-out
Mohammad Salehi Fashami, Jayasimha Atulasimha and Supriyo Bandyopadhyay

This content was downloaded from IP address 143.107.135.170 on 11/07/2023 at 22:44

Nanotechnology **22** (2011) 275708 (9pp) doi:10.1088/0957-4484/22/27/275708

Size effects on silver nanoparticles' properties

F D Kiss[1], R Miotto[2] and A C Ferraz[1]

[1] Instituto de Física da Universidade de São Paulo, Caixa Postal 66318, CEP 05315-970, São Paulo, SP, Brazil
[2] Centro de Ciências Naturais e Humanas, Universidade Federal do ABC, Rua Santa Adelia 166, CEP 09210-170, Santo André, SP, Brazil

Received 10 January 2011, in final form 27 April 2011
Published 20 May 2011
Online at stacks.iop.org/Nano/22/275708

Abstract
In this work a systematic study of the dependence of the structural, electronic, and vibrational properties on nanoparticle size is performed. Based on our total energy calculations we identified three characteristic regimes associated with the nanoparticle's dimensions: (i) below 1.5 nm (100 atoms) where remarkable molecular aspects are observed; (ii) between 1.5 and 2.0 nm (100 and 300 atoms) where the molecular behavior is influenced by the inner core crystal properties; and (iii) above 2.0 nm (more than 300 atoms) where the crystal properties are preponderant. In all considered regimes the nanoparticle's surface modulates its properties. This modulation decreases with the increasing of the nanoparticle's size.

(Some figures in this article are in colour only in the electronic version)

1. Introduction

Science on the nanometric scale has received special attention due to the variety of new properties and applications in physics, chemistry, and biomedicine [1]. It is well established that nanosystem's properties are very distinct from those observed for bulk systems especially due to electron confinement and surface effects [2]. In nanoparticles where the number of atoms on surface is comparable to the total number of atoms, these surface atoms play a decisive role in their catalytical, optical and electromagnetic properties [3, 2, 4, 5]. Catalytical properties make metallic nanoparticles a system of choice in many biological applications, such as drug delivery, biosensors, and microbial agent [6, 7]. This variety of applications had great impact in the medical area, especially in the combat of different diseases caused by bacteria and viruses, and also in cancer treatment [8–11].

The variety of applications and the technological importance made the study of metallic nanoparticles (NPs) a growing research area. While new NP synthetic routes and characterization processes might take large periods, an alternative efficient way to explore this field is the use of theoretical tools. In particular, first-principles calculations of many-electron systems have demonstrated satisfactory agreement with experimental data [2, 12]. However, these calculations are only feasible for small systems. Large structures always need some approximations, as simulation time scales increase rapidly with the structure's size. Among many different approaches, density functional theory (DFT) is one of the most popular theoretical frameworks, mainly due to the good agreement with experimental data combined with the low computational cost if compared to traditional first principle methods based on many-electron wavefunctions.

Besides its multiple uses and some theoretical attempts, there is a lack of systematic studies where size effects on the properties of semiconductor nanoparticles are investigated. Our aim in this work is to evaluate size effects for different nanoparticle models observed in the literature, with a view to contributing to the establishment of a systematic approach for constructing representative nanoparticles to be used in different simulations. For doing so, we employed first-principles DFT calculations, as discussed below.

2. Theoretical modeling

In the following discussion, the term nanoparticle applies to any cluster or agglomerate of atoms, regardless of its size or shape. Nanoparticles are modeled in the supercell scheme, with a vacuum region greater than 10 Å. The ionic potentials are described by ultra-soft pseudopotentials [13–15] and the electron–electron exchange–correlation interactions are described within DFT considering the generalized gradient approximation proposed by Perdew and Wang (PW91) [16].

 © 2011 IOP Publishing Ltd Printed in the UK & the USA

Spin polarization effects, as considered in the Vienna *Ab initio* Simulation Package (VASP) [17, 18], are explicitly treated. The single-particle orbitals are expressed in a plane wave basis with energy up to 200 eV, considering only the Γ-point inside the Brillouin zone. Increasing the number of **k**-points or the basis set results in changes in total energies, atomic distances, and vibrational modes smaller than 0.1%, 0.2%, and 1.0%, respectively. The atoms are assumed to be on their low energy position when the forces are smaller than 10 meV $Å^{-1}$. Vibrational loss spectra are calculated as follows: the normal modes and the corresponding frequencies are the solutions of the dynamical problem of the ions driven by the dynamical matrix, or Hessian, that is constructed with the Hellmann–Feynman forces resulting from displacements of the ions from their equilibrium positions. The intensities are derived from the dipole moment of the system calculated for each distorted geometry as proposed by Preuss and co-workers [19, 20].

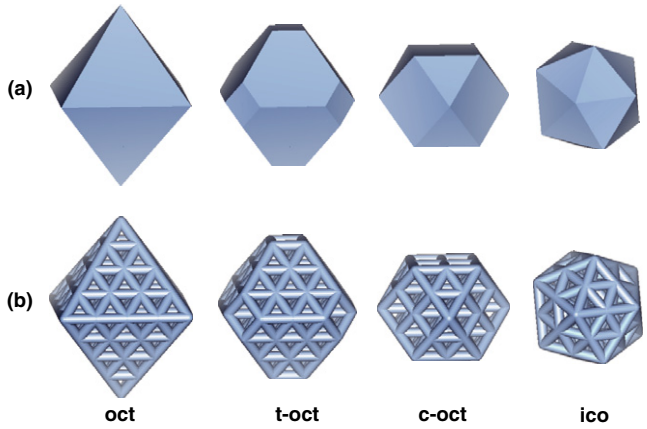

Figure 1. Schematic representation of (a) regular solids and (b) the considered atomic arrangements for the considered nanoparticles. The legend indicates the following structures: octahedral (oct), truncated-octahedral (t-oct), cube-octahedral (c-oct), and icosahedral (ico).

2.1. Nanoparticle's construction

Nanoparticles are synthesized in different sizes and shapes scaling from 1 to 100 nm. In order to take quantum effects into account when calculating atomic structural properties, DFT has proved to be a very precise and reliable method, whose main limitation is related to the size of the treatable structures to be investigated. In order to overcome these intrinsic limitations, it is usual to represent the nanoparticle's surface as a plane surface [11]. Another possibility is to represent the whole nanoparticle by a few atoms [21, 22], or even a single atom [10]. Although simple, these representations lead to results comparable to experimental data [21, 22, 10], especially for vibrational modes. This is because vibrational frequencies are only slightly dependent on the substrate model [23], since they are usually obtained via spring-type methods, where only bond length and atomic masses are crucial parameters. Therefore, small variations in the bond length derived from different substrates will lead to small variations in the vibrational modes and hence in the reasonable agreements usually observed.

It is well known that metallic nanoparticles might be synthesized in different shapes, such as three-dimensional spheres, cubes, octahedra, dodecahedra, or other polyhedra [24–27]. Two-dimensional structures such as triangles, squares and other polygons [28, 29] are also reported. Although many studies suggest that the most stable structure is given by the number of atoms [30–35], other studies indicate that both shape and packaging can be induced by the growth (or synthesis) method [2, 24, 36–39].

Metallic nanoparticles generally follow the FCC or HCP crystal arrangement characteristic of metallic bond systems, with a packing factor of 0.74 with 12 first neighbors [40]. In particular, in the silver crystal, atoms are arranged in a FCC structure and the same is expected for silver based nanoparticles. However, for small clusters there are no restrictions for the crystalline periodicity, and other forms of clustering are allowed. In this case, regular solids, such as icosahedral structures, or non-symmetric systems might be observed [35, 41, 42]. This variety of possible shapes and sizes can make any simulation attempt unfeasible. In order to overcome this issue, in this work we have considered only symmetric nanoparticles. In the following, a given nanoparticle will be identified by its total number of atoms and format. In our discussion, a nanoparticle represents any of the structures studied, regardless of their size or shape. All considered nanoparticles were built considering a FCC crystalline packing in the following: octahedra (oct), truncated-octahedra (t-oct), cube-octahedra (c-oct), and spherical (sph). In addition, the non-crystalline icosahedral (ico) nanoparticle is also considered. A schematic representation of the regular solids and their corresponding atomic structure is shown in figure 1 (the spherical nanoparticles have no regularity on their surface for the different sizes and are not represented).

Our calculated lattice parameter for bulk silver in its FCC structure indicates $a_0 = 4.16$ Å, in good agreement with the experimental value ($a_0 = 4.09$ Å) presented in [43]. All nanoparticles, ranging from 0.3 to 2.9 nm (corresponding to 6 and 561 atoms, respectively), are built considering an extended bulk with the theoretical lattice constant properly cut to give the desired geometry. We believe that our range choice is large enough to provide information on size effects for small nanoparticles and that our conclusions might be extended to larger nanoparticles.

In its bulk crystal structure, silver atoms have coordination 12, i.e. 12 nearest neighbors. In the following discussion, any atoms with coordination smaller than 12 are considered to be surface atoms. From our construction procedure, surface atoms with coordination ranging from 3 to 11 are produced. For simplicity, surface atoms are characterized by their coordination and labeled as cX, where X corresponds to the atoms' coordination number. Examples of different coordinated sites for some of the considered nanoparticles are presented in figure 2.

Bare [001] and [111] surfaces were chosen as the considered nanoparticles present either in one or both surface directions. All surfaces were constructed considering a (1×1)

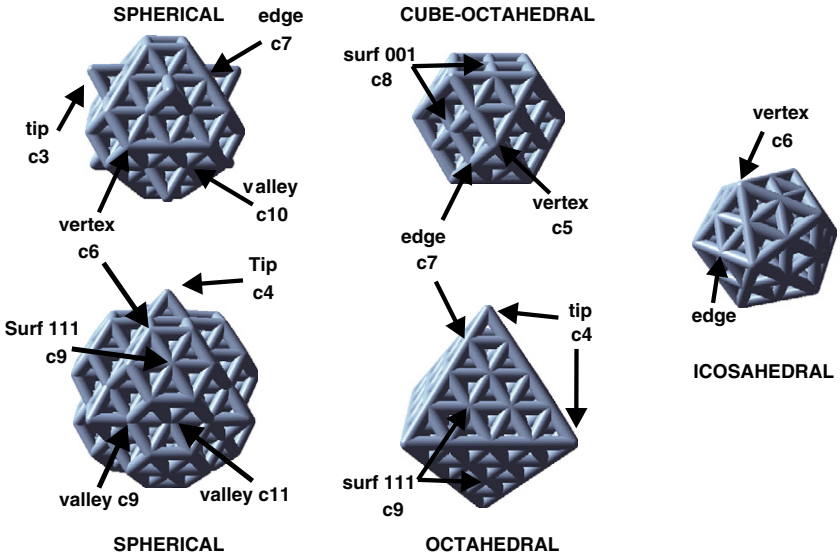

Figure 2. Different coordination sites (cX, where X represents the coordination number) for some of the considered nanoparticles (NPs). The spherical, octahedral, and truncated-octahedral NPs are based on an FCC structure, while the icosahedral NP has no crystalline structure.

Table 1. Mean bond contraction (avg. cont.) observed for a considered atom and its first neighbors with respect to the ideal crystal bond length (2.94 Å). The last column indicates the nanoparticles considered in the averaging. Subsurface, subsubsurface, and inner core (any atom below the subsubsurface layer) c12 atoms are indicated as c12(1), c12(2), and c12(>2), respectively.

Atom	Avg. cont. (%)	Considered nanoparticles
c3	5.9	087
c4	4.8	019, 044, 085, 141 and 146
c5	3.4	013, 043, 055, 147 and 309
c6	2.8	079, 087, 135 and 141
c7	2.1	019, 044, 055, 079, 085, 087, 146, 147 and 309
c8	1.0	043, 055, 135, 147 and 309
c9	0.9	044, 079, 085, 135, 141, 146, 147 and 309
c10	1.4	087
c11	1.4	043, 135 and 141
c12 (1)	1.1	019, 043, 044, 055, 079, 085, 087, 135, 141, 147 and 309
c12 (2)	0.7	055, 079, 085, 087, 135, 141, 147 and 309
c12 (>2)	0.6	079, 085, 087, 135, 141, 147 and 309

reconstruction and six Ag layers. Only the first Ag layer is kept frozen, while the other five layers are allowed to relax. For both surfaces the inner four layers present coordination 12 (c12 atoms) while c8 and c9 atoms characterize the [001] and [111] surfaces, respectively.

3. Results and discussion

Changes in the nanoparticle's properties with increasing size are a consequence of complex combinations of molecular, surface, and crystalline characters. As the number of atoms on the surface grows roughly with the square of the diameter of the nanoparticle ($N_{sup} \propto D^2$) its core grows roughly with the cube of the diameter ($N_{int} \propto D^3$) we expect that the influence of the inner region in the properties of the nanoparticle increases with the diameter. The reduction in the number of surface atoms is clearly seen in figure 3 for different nanoparticle shapes.

Upon relaxation, our first-principles calculations indicated that all nanoparticles kept their original atomic arrangement

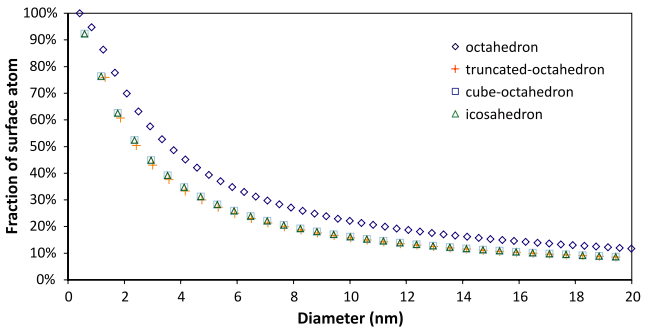

Figure 3. Evolution of the fraction of surface atoms with the nanoparticle's diameter for different shapes. The surface directions for each nanoparticle are indicated in brackets.

(FCC or icosahedral). Bond length contractions are more pronounced for low coordinated atoms, i.e. surface atoms, as clearly seen in table 1. In this table, the average distance of each atom with respect to its first neighbors is compared

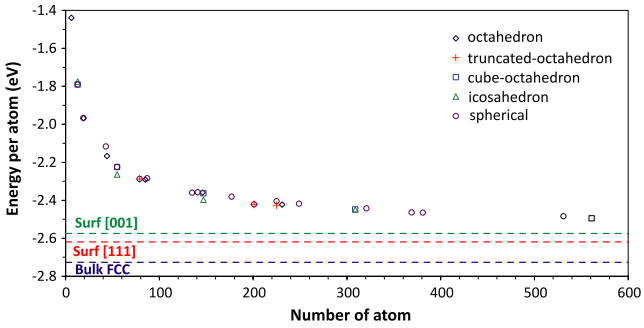

Figure 4. Energy per atom as a function of the nanoparticle's number of atoms. The dashed lines correspond to the energy per atom obtained for ideal crystal, [001], and [111] surfaces, considering an FCC symmetry.

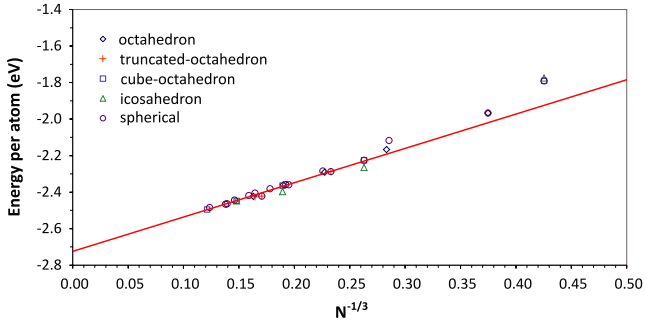

Figure 5. Evolution of energy per atom with the inverse cube root of the number of atoms ($N^{-\frac{1}{3}}$) for the nanoparticles studied. The nanoparticle shapes are indicated. The solid line represents a linear regression for nanoparticles with $N > 100$, with $\varepsilon_{\rm at}^{\rm crystal} = -2.73 + 1.91N^{-\frac{1}{3}}$.

with the interatomic distance of 2.94 Å observed for the ideal crystal. It is also clear from table 1 that bond contraction is directly dependent on the nanoparticle's shape (note that atoms with the same coordination on different shapes present the same contractions). While low coordinated atoms (c3–c7) present the higher contractions, for highly coordinated atoms (c8–c12) this value decreases. It is also interesting to note that for different types of c12 atoms (subsurface, subsubsurface, and inner core indicated in table 1 as c12(1), c12(2), and c12(>2), respectively) the contractions becomes smaller for deeper atoms. This is an indication that for large nanoparticles the inner region has the same configuration as the crystal lattice.

In the next step of our study, we investigate the correlation between the energy per atom of a given nanoparticle with respect to some parameters associated with the size of the nanoparticle. This procedure has the advantage of allowing us to track the system's stability in comparison with other structures, such as the ideal crystal. The energy per atom is computed as

$$\varepsilon_{\rm at} = E_{\rm tot}/N, \tag{1}$$

where $E_{\rm tot}$ and N are the total energy and total number of atoms in the system, respectively. Our total energy calculations suggest that for the nanoparticles considered, the energy per atom decreases continuously when the number of atoms N increases, as clearly seen in figure 4. Most importantly, for large N, $\varepsilon_{\rm at}$ closes the energy per atom calculated for the macroscopic structures considered: the ideal crystal and the [001], [111], and [110] surfaces.

It is clear from figure 4 that for small nanoparticles, the energy per atom variation is much more pronounced. Our data indicate a decrease around 0.85 eV in this range. For nanoparticles between $N = 100$ and 300, the decrease in $\varepsilon_{\rm at}$ is much lower (around 0.14 eV). For larger nanoparticles (between $N = 300$ and 600) changes in the calculated energy per atom are even lower (within 0.05 eV). This behavior of the energy per atom is a first indication of the existence of different nanoparticle regimes: (i) small (up to 100 atoms or 1.5 nm), (ii) intermediate (between 100 and 300 atoms or 1.5 and 2.0 nm), and (iii) large (above 300 atoms or 2.0 nm).

We have also related the energy per atom to the inverse cube root of the total number of atoms ($N^{-\frac{1}{3}}$) for a given nanoparticle, as shown in figure 5. In this case, a linear relation is observed for larger nanoparticles. This is consistent with a scaling law (to first order) with a linear behavior of the type

$$\varepsilon_{\rm at} = a + bN^{-\frac{1}{3}}. \tag{2}$$

The independent term a can be interpreted as the contribution of the inner core to the system's volume and must match the energy per atom obtained for the ideal crystal, since the system tends to bulk silver when $N \to \infty$. The linear regression excludes small nanoparticles (<100 atoms) since they present a small number of c12 atoms, and hence have no crystal-like inner core. The adjusted values are $a = -2.73$ eV and $b = 1.91$ eV. As expected, our fitting indicates an a value in very good agreement with the energy per atom calculated for the silver crystal ($\varepsilon_{\rm at}^{\rm crystal} = -2.73$ eV). A similar linear behavior was obtained by Xie and Blackman [44] within a tight-binding framework. As Xie and Blackman have included small nanoparticles in their fitting, their agreement with the energy per atom of the bulk crystal was less accurate than ours.

The number of c12 atoms in a given nanoparticle can also be used as an indication of its size, as it is directly related to the size of its inner core crystal structure. In this sense, the average coordination number ($\bar{c}$) calculated considering all atoms in a given nanoparticle can also be correlated with the nanoparticle's size, as it will get closer to 12 when the number of atoms in the nanoparticle increases. Figure 6 presents the energy per atom as a function of the average coordination number for all the nanoparticles studied. In addition, we have also included the energy per atom obtained for the ideal silver crystal and for the [001] and [111] silver surfaces. As discussed in section 2, the ideal crystal has only c12 atoms. The [001] and [111] surfaces, on the other hand, are characterized by c8 and c9 atoms and by a central region with four layers of c12 atoms, corresponding to $\bar{c}_{[001]} = 10.67$ and 11.00, respectively. The red line is a linear regression obtained only considering the data obtained for an ideal silver crystal, and the [001] and [111] silver surfaces, i.e. only considering the macrostructures. Therefore, it is fair to say that this linear fitting indicates the limit of the macrostructure regime.

Figure 6 clearly indicates that larger nanoparticles are closer to the linear fit obtained for the macrostructures. In

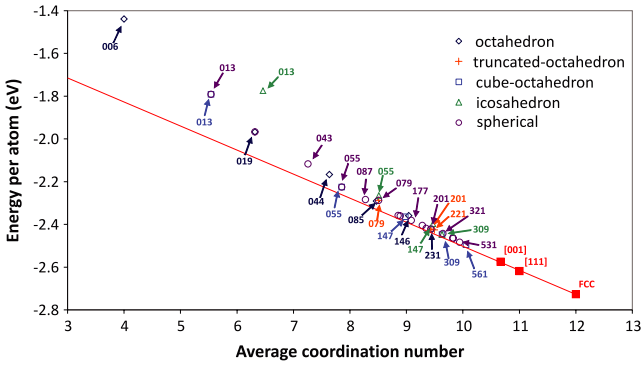

Figure 6. Evolution of energy per atom with the average coordination number in a given nanoparticle. Nanoparticle shapes and structures are indicated. The red squares correspond to the macrostructures: ideal silver crystal, and the [001] and [111] bare surfaces. The solid line corresponds to the linear fit considering only the macrostructures.

contrast, small nanoparticles deviate considerably from this line. In addition, nanoparticles around 150 atoms already present a tendency toward the linear fitting, indicating that this size may represent a transition between the molecular arrangements of small nanoparticles and the bulk-like behavior of larger nanoparticles. Following this assumption, we can again clearly divide the considered nanoparticles into three different groups: (i) small (up to 100 atoms or 1.5 nm), (ii) intermediate (between 100 and 300 atoms, or 1.5 and 2.0 nm), and (iii) large (above 300 atoms or 2.0 nm).

We have next considered the electronic properties of the considered nanoparticles. As indicated in figure 7, for all nanoparticles total charge density plots showed a spherical distribution around the atoms, typical of metal structures. This is consistent with the small structural relaxations observed for all studied nanoparticles. Similarly, our calculated electronic energy levels (not shown) present a typical metal behavior, indicating that the considered nanoparticles kept their metallic character.

Figure 8 represents the total charge distribution around the Fermi level (considering a 0.25 eV window) for different c-oct nanoparticles. Energy levels in this region are chosen since they are strongly correlated to adsorption and surface effects. In addition, their spatial distribution is often used as an indication of the most reactive sites. Our total energy calculations indicate that charge density corresponding to electronic states near the Fermi level are predominantly localized on the surface of the nanoparticle, with small contributions from central regions. For NP 013, for example, these levels are located on c5 surface sites. For NP 055, on the other hand, they are mainly concentrated around c7 sites, while small contributions are seen around c5 and c8 sites.

For larger nanoparticles (NP 147) charge distributions are located around c5, c7, c8, and c9 sites. Thus, our results suggest an increase in regions or sites where functional

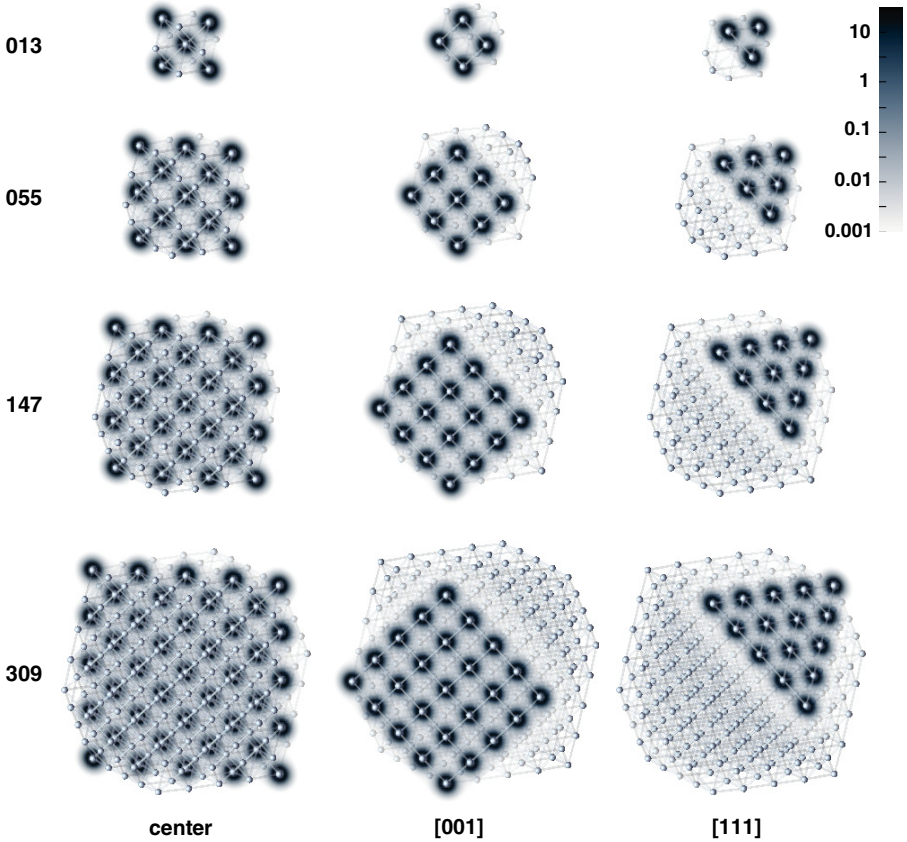

Figure 7. Total charge density distribution for the c-oct 013, 055, 147, and 309 nanoparticles. Planar cuts were made through the center of the nanoparticle and through [001] and [111] surfaces. All charge density contours are in electron $Å^{-3}$.

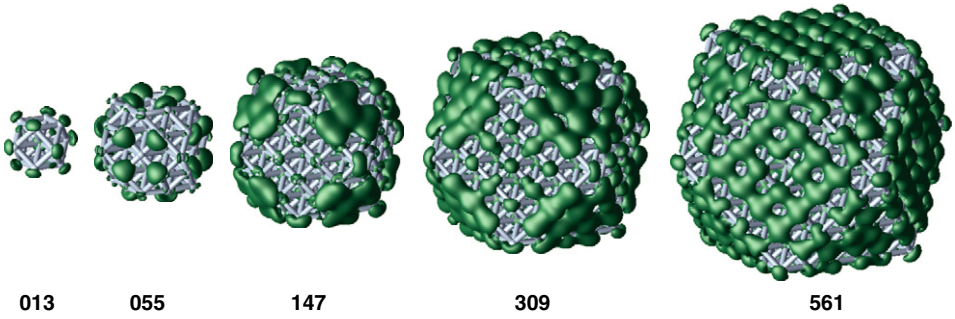

Figure 8. Charge density distribution around the Fermi level for NP c-oct 013, 055, 147, 309, and 561. Charge density contributions were collected considering energy levels within a range of ±0.25 eV around the Fermi level.

groups might be adsorbed in larger nanoparticles. This is a clear indication that the adsorption of different groups on silver nanoparticles is not symmetrically distributed. This is consistent with a recently combined theoretical/experimental study by Castro *et al* [45] where the grafting (surface density of surfactant molecules) on magnetite based nanoparticles is not symmetrically distributed on the nanoparticle's surface. In addition, our data clearly indicate that the study of adsorption processes on metal nanoparticles cannot be restricted to models that do not allow a variety of possible reactive sites in the grafting processes. This is a key issue in the development of drug carriers and biosensors, since in most cases, the surfactants must possess functional groups capable of reacting adequately to the drug to be transported or molecules to be detected.

In order to further access the role of the size of a given nanoparticle in its electronic structure, we systematically compared the density of states (DOS) around the Fermi level for different sizes and shapes of nanoparticles. Selected DOSs, normalized by their respective number of electrons, are represented in figure 9. The molecular character of small nanoparticles (up to 100 atoms or 1.5 nm) is clearly expressed by intense and localized peaks for all considered nanoparticles. When the nanoparticle's size increases, the molecular characteristics in the DOS are reduced and replaced by a mixed behavior modulated by both surface and crystal characters, as indicated for nanoparticles between 100 and 300 atoms (1.5 nm $< D <$ 2.0 nm). For larger nanoparticles (more than 300 atoms or 2.0 nm), surface features are still observed, but the modulation of the ideal crystal becomes dominant, indicating the important role of the inner region in the properties of nanoparticles.

It is worth pointing out that both polyhedral (which preserve the shape with the size) and spherical (that exhibit strong fluctuations in the shape of their surfaces) nanoparticles present similar behavior. This is an indication that this is a general property associated with the size of the nanoparticle. In addition, this interpretation is also consistent with the size regimes observed throughout this work: (i) small (up to 100 atoms or 1.5 nm), (ii) intermediate (between 100 and 300 atoms or 1.5 and 2.0 nm), and (iii) large (above 300 atoms or 2.0 nm). The nanoparticle's inner core is composed by c12 atoms (atoms with coordination 12), a typical crystal environment. As this inner core increases, the predominance of molecular characteristics in the nanoparticle's properties decreases and a transition between both regimes is observed. Surface effects are always present, modulating either the molecular or crystal-like properties, depending on the nanoparticle's size. The larger the nanoparticle, the smaller is the surface modulation.

In the last step of our study, we have addressed the influence of size in the vibrational properties of the system. We conducted a systematic study of vibrational infrared spectra for different nanoparticles, ideal crystal, and bare [001] and [111] surfaces. The loss spectra for the NPs 006, 013, 055, 079, 147, and 309 are shown in figure 10. To set up the dynamical matrix including the inner core influence on the vibrations, we include all atoms of the considered system, i.e. macrostructure or nanoparticle.

The most prominent features in all vibrational spectra are located around 120 cm^{-1} and are bulk related. This is consistent with other theoretical [41] and experimental [46, 47] studies for small silver clusters, where vibrational losses were always found between 16 and 190 cm^{-1}. These results are also consistent with the surface enhanced Raman spectroscopy (SERS) spectra obtained for silver surfaces [48, 49], which do not indicate any losses associated with silver above 300 cm^{-1}. Our results for small nanoparticles (006, 013, 019, and 055) are characterized by distinct and localized peaks, indicating a strong molecular aspect. For larger nanoparticles (079 and 147), a broad loss peak around 115 cm^{-1} is observed. An even broader peak, centered around the same region, is observed for the 309 NP. The identification of a peak around 115 cm^{-1} for nanoparticles with more than 79 atoms indicates that the vibrational properties of larger nanoparticles is clearly dominated by the vibrational properties of the crystal, characterized by a peak at 115 cm^{-1}.

Both [001] and [111] surface spectra are characterized by a peak that is not as broad as the nanoparticle's, but broader than the characteristic bulk peak. This can be seen as an intermediate behavior between these two structural limits (nanoparticle $\leftrightarrow$ crystal). In this sense, the narrowing of the vibrational loss peak can be associated with the structural size of the system: the vibrational spectra resembles more that of an ideal crystal where the number of c12 sites (characteristic of the ideal crystal) increases. Indeed, for the 147 and 309 NPs a small shoulder in the 50 cm^{-1} region is already observed. As this peak is only clearly seen for the ideal crystal, we

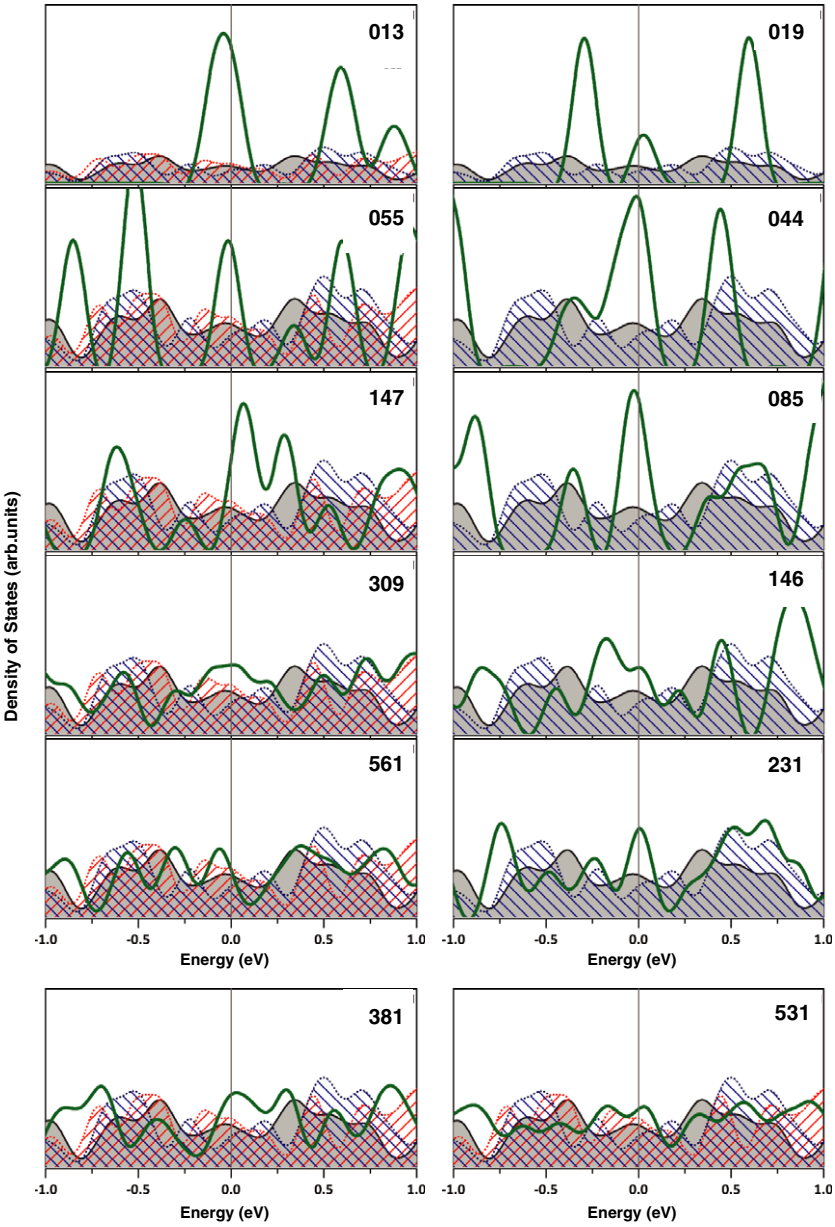

Figure 9. Density of states (DOS) of a given nanoparticle (solid line) compared with the ideal crystal (gray region), the [001] (forward hatched) and [111] (backward hatched) bare surface DOS. Left upper panels: cube-octahedral nanoparticles (013, 055, 147, 309, and 561); right upper panels; octahedral nanoparticles (019, 044, 085, 146, and 231). Lower panels: spherical nanoparticles (381 and 531).

can again infer that our vibrational data are consistent with the size regimes proposed throughout this work: (i) small (up to 100 atoms or 1.5 nm), (ii) intermediate (between 100 and 300 atoms or 1.5 and 2.0 nm), and (iii) large (above 300 atoms or 2.0 nm).

4. Conclusions

In this work a systematic study of dependence of the structural, electronic, and vibrational properties on the nanoparticle's size is performed. Based on our total energy calculations we identified three characteristic regimes directly related to the size of the nanoparticles: (i) strong molecular characteristics for nanoparticles with diameters smaller than 1.5 nm (<100 atoms), (ii) a transient regime with molecular and crystal characteristics for nanoparticles between 1.5 and 2.0 nm (between 100 and 300 atoms), and (iii) a strong crystalline character for nanoparticles larger than 2.0 nm (more than 300 atoms). It is important to mention that in all three regimes surface properties modulate the results. The larger the nanoparticle, the smaller is the surface's modulation in its properties. As these different regimes were identified for nanoparticles with different shapes and structures, we believe that they represent a global behavior.

These regimes are reflected in all investigated properties. Structural properties reflected the importance of c12 sites, as these 12 coordinated atoms characterize the ideal bulk system. The densities of states and energy levels are strongly influenced

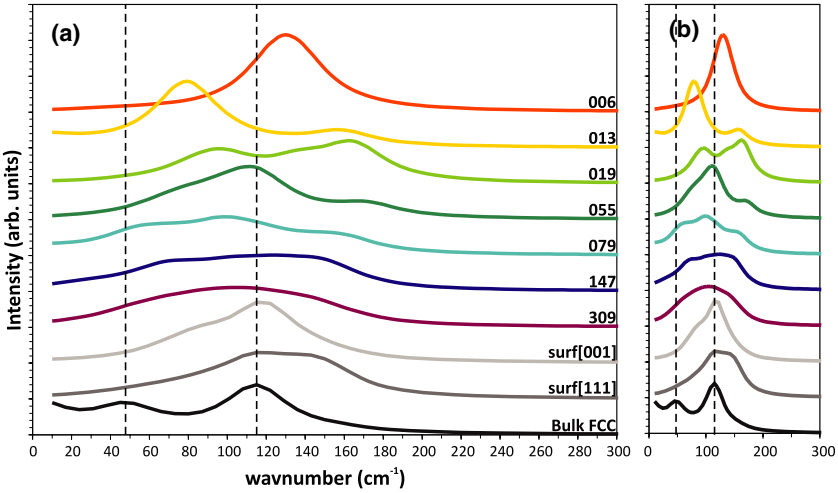

Figure 10. (a) Vibrational spectra of the 006, 013, 019, 055, 079, 147, and 309 NPs, [001] and [111] bare surfaces and ideal bulk silver. (b) Inset with a smaller range to emphasize the characteristic peaks of each structure. As an eye-guide, the dashed lines are placed at the most intense peaks obtained for the ideal silver crystal.

by the size of the nanoparticle, clearly expressing the transition from the molecular to the crystalline regime. The crystalline properties are already dominant for nanoparticles with ±350 atoms. The nanoparticles' vibrational loss spectra present a peak around 115 cm^{-1}, characteristic of the ideal crystal. The secondary 50 cm^{-1}, however, is only observed for larger nanoparticles, suggesting that the transition between different regimes is indeed around 350 atoms.

Acknowledgments

The authors acknowledge financial support from CNPq and FAPESP.

References

[1] Gleiter H 2000 Nanostructured materials: basic concepts and microstructure *Acta Mater.* **48** 1
[2] Burda C, Chen X, Narayanan R and El-Sayed M A 2005 Chemistry and properties of nanocrystals of different shapes *Chem. Rev.* **105** 1025–102
[3] Xu R, Wang D, Zhang J and Li Y 2006 Shape-dependent catalytic activity of silver nanoparticles for the oxidation of styrene *Chem. Asian J.* **1** 888–93
[4] Liz-Marzán L M 2004 Nanometals: formation and color *Mater. Today* **7** 26–31
[5] Mulvaney P 1996 Surface plasmon spectroscopy of nanosized metal particles *Langmuir* **12** 788–800
[6] Skirtach A G, Dejugnat C, Braun D, Susha A S, Rogach A L, Parak W J, Möhwald H and Sukhorukov G B 2005 The role of metal nanoparticles in remote release of encapsulated materials *Nano Lett.* **5** 1371–7
[7] Lee D, Cohen R E and Rubner M F 2005 Antibacterial properties of Ag nanoparticle loaded multilayers and formation of magnetically directed antibacterial microparticles *Langmuir* **21** 9651–9
[8] Qian X, Peng X-H, Ansari D O, Yin-Goen Q, Chen G Z, Shin D M, Yang L, Young A N, Wang M D and Nie S 2008 *In vivo* tumor targeting and spectroscopic detection with surface-enhanced Raman nanoparticle tags *Nat. Biotechnol.* **26** 83–90
[9] Wang J-H and Lin M C 2005 Reactions of trimethylindium on TiO_2 nanoparticles: experimental and computational study *J. Phys. Chem.* B **109** 20858–67
[10] Cho K-H, Choo J and Joo S-W 2005 Surface-enhanced Raman scattering and density functional theory calculation of uracil on gold and silver nanoparticle surfaces *Spectrochim. Acta* A **61** 1141–5
[11] Andreoni W, Grönbeck H and Curioni A 2000 Density functional theory approach to thiols and disulfides on gold: Au(111) surface and clusters *Int. J. Quantum Chem.* **80** 598–608
[12] Baletto F and Ferrando R 2005 Structural properties of nanoclusters: energetic, thermodynamic, and kinetic effects *Rev. Mod. Phys.* **77** 371
[13] Vanderbilt D 1985 Optimally smooth norm-conserving pseudopotentials *Phys. Rev.* B **32** 8412–5
[14] Vanderbilt D 1990 Soft self-consistent pseudopotentials in a generalized eigenvalue formalism *Phys. Rev.* B **41** 7892–5
[15] Kresse G and Joubert D 1999 From ultrasoft pseudopotentials to the projector augmented-wave method *Phys. Rev.* B **59** 1758–75
[16] Perdew J P, Chevary J A, Vosko S H, Jackson K A, Pederson M R, Singh D J and Fiolhais C 1992 Atoms, molecules, solids, and surfaces: applications of the generalized gradient approximation for exchange and correlation *Phys. Rev.* B **46** 6671–87
[17] Kresse G and Furthmüller J 1996 Efficient iterative schemes for *ab initio* total-energy calculations using a plane-wave basis set *Phys. Rev.* B **54** 11169–86
[18] Kresse G and Furthmüller J 1996 Efficiency of *ab initio* total energy calculations for metals and semiconductors using a plane-wave basis set *Comput. Mater. Sci.* **6** 15
[19] Preuss M and Bechstedt F 2006 Vibrational spectra of ammonia, benzene, and benzene adsorbed on Si(001) by first principles calculations with periodic boundary conditions *Phys. Rev.* B **73** 155413
[20] Preuss M, Miotto R, Bechstedt F, Rada T, Richardson N V and Schmidt W G 2006 Structure, energetics, and vibrational spectra of perylene adsorbed on Si(001): first-principles calculations compared with stm and hreels *Phys. Rev.* B **74** 115402
[21] Bertin V, Agacino E, López-Rendon R and Poulain E 2006 The co chemisorption on some active sites of pd clusters: a dft study *J. Mol. Struct.: Theochem.* **769** 243–8

[22] Diaz D, Robles J, Ni T, Castillo-Blum S-E, Nagesha D, Alvarez-Fregoso O-J and Kotov N A 1999 Surface modification of cds nanoparticles with mos42-: a case study of nanoparticle-modifier electronic interaction *J. Phys. Chem.* B **103** 9859–66
[23] Srivastava G P 1990 *The Physics of Phonons* (Bristol: Hilger)
[24] Akhavan O 2009 Silver nanocube crystals on titanium nitride buffer layer *J. Phys. D: Appl. Phys.* **42** 105305
[25] Martin T P 1996 Shells of atoms *Phys. Rep.* **273** 199–241
[26] Roduner E 2006 Size matters: why nanomaterials are different *Chem. Soc. Rev.* **35** 583–92
[27] Marks L D 1994 Experimental studies of small particle structures *Rep. Prog. Phys.* **57** 603
[28] Pal S, Tak Y K and Song J M 2007 Does the antibacterial activity of silver nanoparticles depend on the shape of the nanoparticle? A study of the gram-negative bacterium Escherichia coli *Appl. Environ. Microbiol.* **73** 1712–20
[29] Mock J J, Barbic M, Smith D R, Schultz D A and Schultz S 2002 Shape effects in plasmon resonance of individual colloidal silver nanoparticles *J. Chem. Phys.* **116** 6755–9
[30] Schooss D, Blom M N, Parks J H, Issendorff B V, Haberland H and Kappes M M 2005 The structures of Ag_{55}^{+} and Ag_{55}^{-}: trapped ion electron diffraction and density functional theory *Nano Lett.* **5** 1972–7
[31] Jennison D R, Schultz P A and Sears M P 1997 *Ab initio* calculations of Ru, Pd, and Ag cluster structure with 55, 135, and 140 atoms *J. Chem. Phys.* **106** 1856–62
[32] Blom M N, Schooss D, Stairs J and Kappes M M 2006 Experimental structure determination of silver cluster ions (Ag(n)+, 19 $<$ or $=$ n $<$ or $=$ 79) *J. Chem. Phys.* **124** 244308
[33] Doye J P K and Wales D J 1998 Global minima for transition metal clusters described by Sutton–Chen potentials *New J. Chem.* **22** 733–44
[34] Häkkinen H, Moseler M, Kostko O, Morgner N, Hoffmann M A and Issendorff B V 2004 Symmetry and electronic structure of noble-metal nanoparticles and the role of relativity *Phys. Rev. Lett.* **93** 093401
[35] Poteau R and Spiegelmann F 1993 Structural properties of sodium microclusters (n = 4–34) using a Monte Carlo growth method *J. Chem. Phys.* **98** 6540–57
[36] Sun Y and Xia Y 2002 Shape-controlled synthesis of gold and silver nanoparticles *Science* **298** 2176–9
[37] Koski K J, Kamp N M, Smith R K, Kunz M, Knight J K and Alivisatos A P 2008 Structural distortions in 5–10 nm silver nanoparticles under high pressure *Phys. Rev.* B **78** 165410
[38] Kan C-X, Zhu J-J and Zhu X-G 2008 Silver nanostructures with well-controlled shapes: synthesis, characterization and growth mechanisms *J. Phys. D: Appl. Phys.* **41** 155304
[39] Maliszewska I, Szewczyk K and Waszak K 2009 Biological synthesis of silver nanoparticles *J. Phys.: Conf. Ser.* **146** 012025
[40] Kittel C 2004 *Introduction to Solid State Physics* (New York: Wiley)
[41] Poteau R, Heully J-L and Spiegelmann F 1997 Structure, stability, and vibrational properties of small silver cluster *Z. Phys.* D **40** 479–82
[42] Huda M N and Ray A K 2003 Electronic structures and magic numbers of small silver clusters: a many-body perturbation-theoretic study *Phys. Rev.* A **67** 013201
[43] Methfessel M, Hennig D and Scheffler M 1992 Trends of the surface relaxations, surface energies, and work functions of the 4d transition metals *Phys. Rev.* B **46** 4816–29
[44] Xie Y and Blackman J A 2001 Transferable tight-binding model for palladium and silver *Phys. Rev.* B **64** 195115
[45] Castro L L, Gonçalves G R R, Skeff Neto K, Morais P C, Bakuzis A F and Miotto R 2008 Role of surfactant molecules in magnetic fluid: comparison of Monte Carlo simulation and electron magnetic resonance *Phys. Rev.* E **78** 061507
[46] Haslett T L, Bosnick K A and Moskovits M 1998 Ag_5 is a planar trapezoidal molecule *J. Chem. Phys.* **108** 3453–7
[47] Bosnick K A, Haslett T L, Fedrigo S, Moskovits M, Chan W-T and Fournier R 1999 Tricapped tetrahedral Ag_7: a structural determination by resonance Raman spectroscopy and density functional theory *J. Chem. Phys.* **111** 8867–70
[48] Nie S and Emory S R 1997 Probing single molecules and single nanoparticles by surface-enhanced Raman scattering *Science* **275** 1102–6
[49] Doering W E and Nie S 2002 Single-molecule and single-nanoparticle SERS: examining the roles of surface active sites and chemical enhancement *J. Phys. Chem.* B **106** 311–7